

THE EFFECT OF VISCOSITY ON TURBULENT MIXING IN A CO-FLOWING JET MIXER

Gokul Pathikonda

The George W. Woodruff School
of Mechanical Engineering
Georgia Institute of Technology, Atlanta

Mustafa Usta

The George W. Woodruff School
of Mechanical Engineering
Georgia Institute of Technology, Atlanta

Cameron Ahmad

The George W. Woodruff School
of Mechanical Engineering
Georgia Institute of Technology, Atlanta

Vincent Lee

The George W. Woodruff School
of Mechanical Engineering
Georgia Institute of Technology, Atlanta

Irfan Khan

Dow Chemical, Lake Jackson, TX

Paul Gillis

Dow Chemical, Lake Jackson, TX

Devesh Ranjan

The George W. Woodruff School
of Mechanical Engineering
Georgia Institute of Technology, Atlanta
devesh.ranjan@me.gatech.edu

Cyrus Aidun

The George W. Woodruff School
of Mechanical Engineering
Georgia Institute of Technology, Atlanta
cyrus.aidun@me.gatech.edu

ABSTRACT

Turbulent shear-driven mixing in a coaxial and co-flowing configuration is studied experimentally and computationally to understand and model the effect of viscosity gradients in the flow field. Two liquids with a large disparity in dynamic viscosity are mixed, with a low viscosity liquid injected as a high-velocity inner jet into a high viscosity co-flowing outer flow. Simultaneous experimental measurements of the velocity and concentration fields are made using high-resolution PIV and PLIF to obtain their turbulent cross-correlation statistics for viscosity ratios of 1 and 40. LES simulations are also performed using various mixture subgrid-scale (SGS) to investigate the effectiveness of the same in predicting the scalar mixing and to complement the experimental observations. We aim to understand the effect viscosity gradients in the flow have on turbulent mixing at high Schmidt (Sc) and Reynolds numbers (Re). The preliminary experimental and computational results already show a stark difference in the flow structure.

INTRODUCTION

The turbulent mixing between two liquids of different viscosities is an extremely common phenomenon in nature and in engineering applications. A few examples of significance that involve heterogeneous fluid mixing would in-

clude the mixing of paints, fuel-air mixtures, food processing, industrial mixing of chemicals etc. These phenomena in liquids at very high Sc result in a large range of dynamically significant scalar and velocity scales. Further, viscosity variations have a profound and unexpected effect on flow stability, turbulent cascade associated with the mean energy dissipation rate, and characteristics of entrainment in mixing. The viscous stress term will depend on the gradient of viscosity, ∇v , in addition to the magnitude of local viscosity, v . The extra term, $\nabla v \cdot [\nabla u + (\nabla u)^T]$, in the momentum equation profoundly alters the viscous stress field.

The flow of fluids with viscosity variation alters turbulence characteristics at a fundamental level. For high Reynolds number turbulent flow, the small scales are uniquely dependent on kinematic viscosity and mean energy dissipation rate. Furthermore, viscosity is assumed to be a 'small-scale' quantity without significant effect on scales in the inertial range. This is obviously not the case for heterogeneous turbulent flows mixing fluids with different viscosity. Two extra terms appear due to viscosity variation at high Re in the one-point kinetic energy budget equations. These terms act as a source and sink in the turbulent kinetic energy budget, and thus have a significant effect on the entrainment and reaction characteristics. To provide a meaningful evaluation of these terms in different flows and different flow regimes, velocity and viscosity gradients

are to be determined simultaneously at the same spatial location. Mixing of fluids with large viscosity difference in the transition region where the flow is not fully turbulent may cause additional complexities. Direct numerical simulation (DNS) in conjunction with experiments is required to provide this information both during transition and for fully turbulent flows up to the maximum Reynolds number possible. However, DNS is only possible for low Reynolds number and not possible for reacting liquids because of the large Schmidt number (Sc). The relevant flow parameters for mixing of a co-axial jet are the effective Reynolds number, Re_e , which represents the same parameter for a single jet with the same effective momentum as the coaxial jet; the local turbulent Reynolds number, Re_λ , based on root-mean-square of velocity, $RMS(u)$ and the Taylor length scale, λ ; and the total Reynolds number, Re_t , based on the ratio of inertia, $u \cdot \nabla u$, to the sum of the two viscous and viscous gradient stress terms, $\overline{\nabla v \cdot [\nabla u + (\nabla u)^T]} + \nu \nabla^2 u$. To examine the effect of viscosity variation on energy dissipation and mixing, two-point correlations estimated based on the results from computational simulations and experimental measurements can be considered.

In the current study, we employ simultaneous PIV and PLIF at high resolutions for experimental data at high Re . Similarly, LES simulations are also performed to study the effects of viscosity gradient terms in the process of mixing, and to develop the appropriate mixing model that accurately considers these gradients. Preliminary data from these two-pronged investigations have shown already a clear change in the structure of turbulent mixing and scalar transport that emphasizes the effect of disparate viscosities in the flow. These agree with the observations made previously by Talbot *et al.* (2013), albeit at low Sc -flows.

METHODOLOGY

Experiments

The current experiments on turbulent mixing of flows of different viscosity are investigated using the Viscous Mixing Jet facility within the Shock Tube and Advanced Mixing Laboratory (STAML) at Georgia Institute of Technology. The system produces a 10mm diameter jet in a 52mm-diameter co-flowing stream inside of a pipe. The two streams are independently driven by a pressured tank capable of housing 800 litres of each liquid and rated to driving pressures of upto 125 *PSI*. The flow rates are measured using Omega FDT-40 ultrasonic flow meters, and are maintained constant using PID controlled 2 in 24000SVF-54-3661 globe control valves. The outer stream passes through an 8 in NPT settling chamber containing flow conditioning grids and honeycombs, before converging into the 52mm test section. Inner flow flows through an ~ 80 -diameter straight pipe section before interacting with the outer stream in the test section. The test section itself is 1.5 m-long, made with a clear 2 in NPT-acrylic pipe, before the mixed flow enters the dump-tanks. This pump-less system is capable of obtaining steady and high flow rates of viscosities up to 1000 *Pa · s*.

To investigate the turbulent mixing of the two streams, simultaneous PIV and PLIF are used to measure turbulent velocity fields and scalar transport respectively. For PIV, both the fluid streams are seeded with 10 μm hollow glass spheres. Further, 1.3×10^{-4} g/L of Rhodamine 6G dye is added to the outer stream to enable fluorescence imaging of the liquid as it mixes with the inner fluid. A thin 532nm

laser sheet of ≈ 1 mm width is formed from the output of a Litron PIV-Nano 120-15 Nd-YAG laser, and is used for mie-scattering of PIV particles and excitation of the Rhodamine dye at the center-plane of the test section. This illuminated field-of-view is imaged simultaneously by two 29MP TSI PowerView cameras viewing through a 50 : 50 beam splitter. Using a calibration image of a dense rectangular grid taken before the experiment, the images from the two cameras are mapped on to the same physical space. To avoid the cross talk of the narrow-band PIV light scatter and a broadband PLIF signal between the two cameras, the PIV camera is fitted with a 532nm bandpass filter (6nm FWHM) and the PLIF camera is fitted with a 532nm notch filter (6nm FWHM, OD 6). The field-of-view has dimensions of ≈ 50 mm \times 80 mm, and to investigate the long evolution along the pipe, the entire system is translated to multiple downstream locations. At each location, around 250 time-uncorrelated snapshots (at 1 Hz) of flow are captured and measurements are ensemble averaged for statistical descriptions. The final PIV vector processing was done on LaVision Davis software, with a final 24 px \times 24 px interrogation spot size and vector spacing of 425 μm . The PLIF processing was performed in-house under the optically thin assumption, and has a final in-plane resolution of 23 μm .

Two sets of experiments are presented in the current study, highlighting the effect of viscosity ratio, m on the turbulent evolution and mixing of the streams. The first experiment ('*case-m1*') studies the baseline case of $m = 1$ (constant viscosity mixing), where both the streams comprise of water. This is a classical jet in a confined co-flow, that has previously been investigated, among others, by (Talbot *et al.*, 2013; Chorny & Zhdanov, 2012; Lima *et al.*, 2002, etc.). Additionally, a second $m = 40$ experiment ('*case-m40*') was conducted by sending a viscous liquid in outer, co-flowing stream. The viscosity of the liquid in outer stream is increased by adding 12 g/L by weight of Sodium Carboxy Methyl Cellulose (Na-CMC) additive. The CMC solution at these concentrations have previously been shown to have a predominantly Newtonian behavior. Table 1 lists the flow conditions at which the current experiments were performed. The Reynolds numbers are calculated using the respective diameters. Under these conditions, the Komogorov and Batchelor length scale are estimated to be 50 μm and 1.6 μm respectively.

Large Eddy Simulations

To study the turbulent mixing between two fluids of different viscosities accurately, large-eddy simulation (LES) are conducted for the cases listed in Table 1. In addition to the Navier-Stokes equations, a transport equation is solved for mixture fraction (conserved scalar, ξ). The filtered governing equations reads;

$$\frac{\partial \tilde{u}_i}{\partial x_i} = 0 \quad (1)$$

$$\frac{\partial \tilde{u}_i}{\partial t} + \tilde{u}_j \frac{\partial \tilde{u}_i}{\partial x_j} = -\frac{1}{\rho} \frac{\partial \tilde{p}}{\partial x_i} + \frac{\partial}{\partial x_j} (\widetilde{2\nu S_{ij}}) - \frac{\partial \tau_{ij}}{\partial x_j} \quad (2)$$

Table 1. Experimental conditions for the two cases discussed in current work

Case Name	Viscosity Ratio, m v_o/v_i	Flow Rate		Reynolds Number, Re_d		Bulk Velocity	
		Jet (Q_i)	Co-flow (Q_o)	Jet (Re_i)	Co-flow (Re_o)	Jet (U_i)	Co-flow (U_o)
Case-m1	1	5.6 lpm	23 lpm	10000	8000	1 m/s	0.2 m/s
Case-m40	40	5.6 lpm	23 lpm	10000	200	1 m/s	0.2 m/s

$$\frac{\partial \tilde{\xi}}{\partial t} + \tilde{u}_j \frac{\partial \tilde{\xi}}{\partial x_j} = \frac{\partial}{\partial x_j} \left[(D + D_t) + \frac{\partial \tilde{\xi}}{\partial x_j} \right] \quad (3)$$

where \tilde{u} is filtered velocity, ρ is density, \tilde{p} is filtered pressure, ν is kinematic viscosity, S_{ij} is strain-rate tensor, τ_{ij} is SGS stress tensor, $\tilde{\xi}$ is filtered mixture fraction, D is molecular diffusion coefficient, and D_t is turbulent diffusion coefficient. We use a box filter for the filtered quantities in the equations.

The computational domain is a cylindrical geometry with a structured mesh similar to that of Tkatchenko *et al.* (2007) and it includes the inner and outer turbulent jet inlet. The length of the domain is 8 times the outer tube diameter. The theoretical turbulent velocity profile imposed at the inlet in computations. The same profile was achieved and measured experimentally. The local mixture viscosity varies linearly with mass fraction of species as experimentally verified, and a pdf. For the LES subgrid-scale model, we implemented Smagorinsky (Smagorinsky (1963)), dynamic Smagorinsky (Germano *et al.* (1991)), and dynamic mixed Smagorinsky (Zang *et al.* (1993)). We found that the dynamic model was better than the Smagorinsky model at predicting the scalar and velocity properties of interest. The dynamic model inherently takes the advantage of dynamic adjustment of model coefficients. So dynamic model is employed for the simulations. Additionally, scalar SGS variance and the mixture fraction are used for a PDF approach to close the SGS fluctuations of viscosity. The simulations are performed on the Texas Advanced Computing Center (TACC)'s Stampede 2 system, using the open-source finite volume method (FVM) solver, OpenFOAM v6. To evaluate the mixing behavior, time-averaged LES predictions, and mean, RMS and variance of flow properties are calculated. Then these findings are compared with experimental measurements.

RESULTS

Evolution of Mean Turbulence

Figure 1a-d shows the comparison between the experimental measurements and LES results via an example snapshot, the mean and turbulent velocity and scalar quantities for *case-m1*. Each sub-figure represents half of the experimental data (*top*) and other half from simulations (*bottom*) of the axisymmetric flow system. Both the resolved and the sub-grid turbulent variances have been added in the comparisons. The excellent agreement between the two approaches highlights the ability of the dynamic model (DM) to accurately capture the mixing dynamics of the flow system. These observations have previously been shown by Zhdanov & Chorny (2011), who have evaluated and compared the effectiveness of various sub-grid models using PLIF measurements. Also shown in figure 1a and 1e is the

increased resolution of the PLIF measurements relative to the simulations, which can be leveraged to develop more effective sub-grid models.

The instantaneous, mean and turbulent quantities from experiments and computations for the variable viscosity mixing can be seen in figure 1e-h. The cross-stream transport of momentum and conserved species is weaker owing to the higher viscosity in the outer stream, higher Schmidt number (Sc), and greater turbulence dissipation. Further, the ability of DM in predicting the dynamics of variable viscosity flows is evident in these observations, where good agreement is seen between the experimental measurements and computational predictions. DM's ability to adjust the model coefficient locally using the resolved strain tensor enables better predictions in the flow conditions where viscosity gradients exist, at least for the Re investigated in the current study.

Structure of Scalar Mixing

The resolution of the current experimental data can be leveraged to investigate the structure of scalar mixing. This is particularly important for applications when the two fluids can react (in a mixing limited reaction) to form a product, and the flow structure dictates the area for the product formation. There are a number of derivative quantities from concentration fields that have been evaluated to study scalar mixing, such as mixedness, mixing-layer width, mixed-mass, mixed-product (X_p), etc. For the current work, we use the definition of latter 'mixed-product mole fraction, X_p ' to study the theoretical mole fraction of the hypothetical product that forms from a fast chemical reaction between the incoming streams. The formation of a 'mixed-product' everywhere is limited by the amount of lean reactant at each location, is defined as Cook & Dimotakis (2001),

$$X_p = \begin{cases} \frac{\xi}{\xi_s} & \text{for } \xi \leq \xi_s \\ \frac{1-\xi}{1-\xi_s} & \text{for } \xi > \xi_s \end{cases} \quad (4)$$

where c_s is the mole fraction for a stoichiometric mixture. X_p goes from 0 (no product formed) to 1 (maximum concentration of formed product) depending on the relative concentrations of the two liquids at each location. Figure 2 shows the instantaneous fields of X_p identifying important structural differences between the two viscosity ratios, and the associated changes in the mean fields. We assume an equimolar stoichiometry, and consequently $\xi_s = 0.5$. Despite the similarities in the velocity statistics seen earlier in figures 1c and 1g, the mixing characteristics between the two flows are vastly different. As expected, this primarily arises from the differences in the Reynolds numbers and in the strong effect of outer stream viscosity in latter case in dissipating small wavenumber eddies. The *case-m1* shows

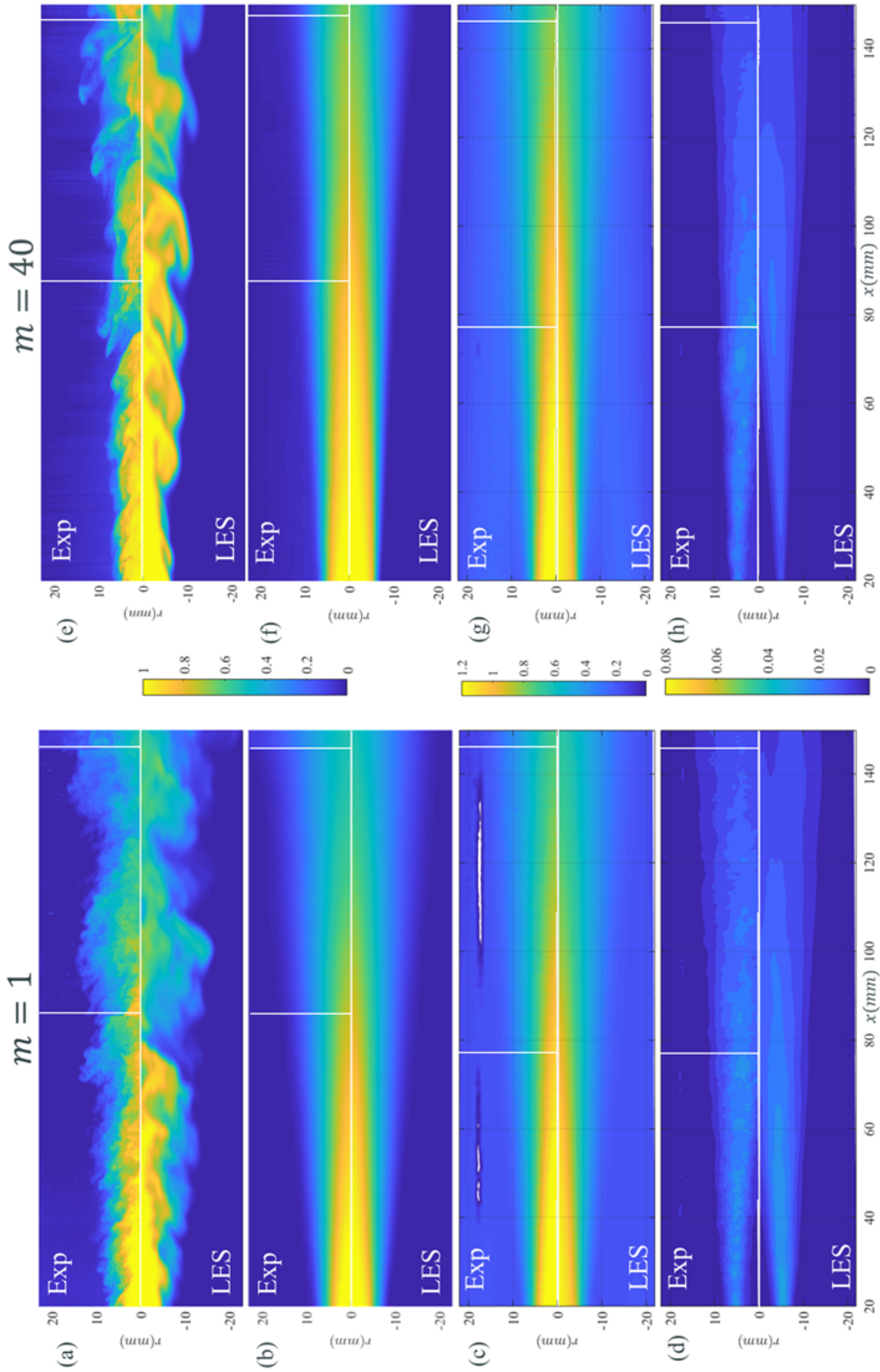


Figure 1. Fields of (a,e) Example scalar snapshots, (b,f) mean scalar concentration fields, (c,g) mean velocity, and (d,h) mean streamwise turbulent kinetic energy of (a-d) *case-m1* and (e-h) *case-m40*.

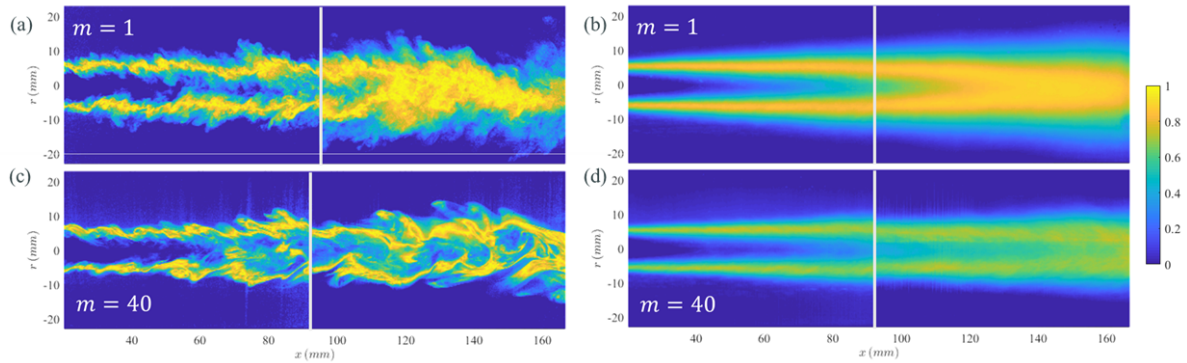


Figure 2. (a,c) An example snapshot and (b,d) average fields of mixed product mole fraction, X_p for (a,b) *case-m1* and (c,d) *case-m40* estimated from the experimental data

a homogeneous production of the product along the interacting shear layers that grow and merge into a jet-like flow at the center of the test section. This however is impeded in *case-m40*, as the viscosity mitigates the formation of the turbulence in the shear layer, with the latter merely undergoing shear-layer instabilities with minimal intermittent transition. The result of this can be seen on the mixing profiles, where ineffective mixing leads to the reduction in the turbulent regions and surface area available for the two fluids to interact with each other.

This stark difference in the structure of mixing has important implications on more engineering-relevant chemistries, which hardly involve simple one-step reactions. For example, we can consider the ‘consecutive-competitive’ reactions, where one of the formed products (R , ‘desired’) continues to react with the initial reactants to form a secondary product (S , ‘undesired’). In such a scenario, the *case-m1* would lead to thorough mixing of the two streams forming the desired product R more selectively, while the *case-m40* would inefficiently produce R only at the interfaces. Subsequent merging of the two shear-layers with unreacted inner liquid would lead to formation of large amounts of secondary, undesired product S . This continuous production of R in the variable viscosity case, and its interaction with the inner stream with potential to produce S is highlighted in the mean profiles of X_p in figure 2. Typically, the large viscosities involved in chemical industrial applications imply that the initial jet momentum and the subsequent shear-generated turbulence eventually dissipate into the laminar outer stream. It is essential to achieve complete turbulent mixing in an effective manner before the eventual decay of velocity fluctuations. For this reason, the evaluation of not only the single point statistics, but also the mixing structure is important to investigate reaction dynamics of the system.

CONCLUSIONS AND FUTURE WORK

The current work presents the preliminary experimental and computational results in studying the structure of turbulent mixing in a variable viscosity environment. Particularly, the evolution of the mixing using high resolution PLIF, implications on reacting flows and the considerations for modeling are discussed here. Comparisons of mean and turbulent velocities and spreading of the scalar jet between the experiments and computations show good agreement for both viscosity ratios of 1 and 40. As expected, the constant viscosity jet ($m = 1$) spreads faster, with enhanced

mixing compared to variable viscosity jet ($m = 40$). This tends support to the dynamic model (DM) used in predicting the same. The mean behavior is a combination of the effects of Reynolds number (higher viscosity having a lower Reynolds number) and effects of variable viscosity fields. The differences in mixing behavior have been shown using the mixed product molar concentration (X_p) that aids in visualizing the effects of the same on reacting flows. The effectiveness of initial mixing of the two streams (or lack thereof), dictates the yield of a broad class of reactions, such as mixing-limited, consecutive-competitive reactions.

The effectiveness of DM in predicting the turbulent mixing of constant viscosity and variable viscosity flows has also been demonstrated for the current Re and viscosity ratios. Dynamic model accurately alters the model coefficient in accordance with the local strain-rate tensor and thus it becomes a valid closure model for variable viscosity as well as constant viscosity.

ACKNOWLEDGMENT

This project is funded by Dow through the University Project Initiative. This work also used the Extreme Science and Engineering Discovery Environment (XSEDE) for computational need, which is supported by National Science Foundation grant number TG-CTS100012. Specifically, we used the Stampede2 system at the Texas Advanced Computing Center (TACC).

REFERENCES

- Chorny, Andrei & Zhdanov, Valery 2012 Turbulent mixing and fast chemical reaction in the confined jet flow at large schmidt number. *Chemical engineering science* **68** (1), 541–554.
- Cook, Andrew W & Dimotakis, Paul E 2001 Transition stages of rayleigh–taylor instability between miscible fluids. *Journal of Fluid Mechanics* **443**, 69–99.
- Germano, Massimo, Piomelli, Ugo, Moin, Parviz & Cabot, William H 1991 A dynamic subgrid-scale eddy viscosity model. *Physics of Fluids A: Fluid Dynamics* **3** (7), 1760–1765.
- Lima, MMCL, Palma, JMLM & Areal, PM 2002 Mixing in coaxial confined jets of large velocity ratio. In *Proc. of 11th Int. Symp. on Appl. of Laser Techniques to Fluid Mechs.*
- Smagorinsky, JS 1963 General circulation model of the atmosphere. *Mon. Weather Rev* **91**, 99–164.

- Talbot, B, Danaila, L & Renou, B 2013 Variable-viscosity mixing in the very near field of a round jet. *Physica Scripta* **2013** (T155), 014006.
- Tkatchenko, Igor, Kornev, Nikolai, Jahnke, Steffen, Steffen, Günter & Hassel, Egon 2007 Performances of les and rans models for simulation of complex flows in a coaxial jet mixer. *Flow, turbulence and combustion* **78** (2), 111–127.
- Zang, Yan, Street, Robert L & Koseff, Jeffrey R 1993 A dynamic mixed subgrid-scale model and its application to turbulent recirculating flows. *Physics of Fluids A: Fluid Dynamics* **5** (12), 3186–3196.
- Zhdanov, Valery & Chorny, Andrei 2011 Development of macro-and micromixing in confined flows of reactive fluids. *International Journal of Heat and Mass Transfer* **54** (15-16), 3245–3255.